Polarized thermal radiation by layer-by-layer metallic emitters with sub-wavelength grating

Jae-Hwang Lee[1*], Wai Leung[1], Tae Guen Kim[2], Kristen Constant[1] and Kai-Ming Ho[1]

[1]Ames Laboratory U.S .DOE, Iowa State University, Ames, IA, 50011, USA
[2]Department of Electronics Engineering, Korea University, Seoul 136-701, South Korea
*Corresponding author: leejh@iastate.edu

Metallic thermal emitters consisting of two layers of differently structured nickel gratings on a homogeneous nickel layer are fabricated by soft lithography and studied for polarized thermal radiation. A thermal emitter in combination with a sub-wavelength grating shows a high extinction ratio, with a maximum value close to 5, in a wide mid-infrared range from 3.2 to 7.8 µm, as well as high emissivity up to 0.65 at a wavelength of 3.7µm. All measurements show good agreement with theoretical predictions. Numerical simulations reveal that a high electric field exists within the localized air space surrounded by the gratings and the intensified electric-field is only observed for the polarizations perpendicular to the top sub-wavelength grating. This result suggests how the emissivity of a metal can be selectively enhanced at a certain range of wavelengths for a given polarization.

OCIS codes: (030.5620) Radiative transfer; (230.5298) Photonic crystals; (230.5440) Polarization-selective devices

References and links

1. A. Heinzel, V. Boerner, A. Gombert, B. Bläsi, V. Wittwer, and J. Luther, "Radiation filters and emitters for the NIR based on periodically structured metal surfaces," J. Mod. Opt. **47**, 2399-2419 (2000).
2. M. U. Pralle, N. Moelders, M. P. McNeal, I. Puscasu, A. C. Greenwald, J. T. Daly, E. A. Johnson, T. George, D. S. Choi, I. El-Kady, and R. Biswas, "Photonic crystal enhanced narrow-band infrared emitters," Appl. Phys. Lett. **81**, 4585-4587 (2002).
3. S. Y. Lin, J. Moreno, and J. G. Fleming, "Three-dimensional photonic-crystal emitter for thermal photovoltaic power generation," Appl. Phys. Lett. **83**, 380-382 (2003).
4. H. Sai, Y. Kanamori, and H. Yugami, "High-temperature resistive surface grating for spectral control of thermal radiation," Appl. Phys. Lett. **82**, 1685-1687 (2003).
5. J.-H. Lee, Y.-S. Kim, K. Constant, and K.-M. Ho, "Woodpile metallic photonic crystals fabricated by using soft lithography for tailored thermal emission," Adv. Mater. **19**, 791-794 (2007).
6. P. J. Hesketh, J. N. Zemel, and B. Gebhart, "Polarized spectral emittance from periodic micromachined surface. I. Doped silicon: The normal direction," Phys. Rev. B **37**, 10795-10802 (1988).
7. F. Marquier, M. Laroche, R. Carminati, J.-J. Greffet, "Anisotropic polarized emission of a doped silicon lamellar grating," J. Heat Trans. **129**, 11 (2007).
8. J. C. W. Lee and C. T. Chan, "Circularly polarized thermal radiation from layer-by-layer photonic crystal structures," Appl. Phys. Lett. **90**, 051912 (2007).
9. S. Ingvarsson, L. J. Klein, Y.-Y. Au, J. A. Lacey, and H. F. Hamann, "Enhanced thermal emission from individual antenna-like nanoheaters," Opt. Express **15**, 11249 (2007).
10. T. Saito, L. R. Hughey, J. E. Proctor, and T. R. O'Brian, "Polarization characteristics of silicon photodiodes and their dependence on oxide thickness," Rev. Sci. Instrum. **67**, 3362 (1996).
11. N. P. Camacho, P. West, P. A. Torzilli, and R. Mendelsohn, "FTIR microscopic imaging of collagen and proteoglycan in bovine cartilage," Biopolymers **62**, 1-8 (2001).
12. H. Arimoto, "Multispectral polarization imaging for observing blood oxygen saturation in skin tissue," Appl. Spectrosc. **60**, 459-464 (2006).
13. E.W. Thulstrup and J. Michl, *Elementary Polarization Spectroscopy* (VCH, New York, 1989), Chap. 3.
14. A. G. Worthing, "Deviation from Lambert's law and polarization of light emitted by incandescent tungsten, tantalum and molybdenum and changes in the optical constants of tungsten with temperature," J. Opt. Soc. Am. **13**, 635-650 (1926).
15. O. Sandus, "A review of emission polarization," Appl. Opt. **4**, 1634-1642 (1965).
16. J.-H. Lee, J.C.W. Lee, W. Leung, M. Li, K. Constant, C. T. Chan, and K.-M. Ho, "Polarization engineering of thermal radiation using metallic photonic crystals," Adv. Mater. (to be published).

17. J.-H. Lee, C.-H. Kim, K. Constant, and K.-M. Ho, "Two-polymer microtransfer molding for highly layered microstructures," Adv. Mater. **17**, 2481-2485 (2005).
18. J. B. Pendry, "Photonic band structures," J. Mod. Opt. **41**, 209-229 (1994).
19. Z.-Y. Li and L.-L. Lin, "Photonic band structures solved by a plane-wave-based transfer-matrix method," Phys. Rev. E **67**, 046607 (2003).
20. D. W. Lynch and W. R. Hunter, "Nickel (Ni)" in *Handbook of Optical Constants of Solid,* E.D. Palik, ed. (Academic, London, 1985).
21. Y. S. Touloukian and D. P. DeWitt, *Thermal Radiative Properties: Metallic Elements and Alloys* (IFI/Plenum, New York, 1970).

1. Introduction

Thermal radiation (TR) properties of materials have been rigorously studied because of the importance of TR in various scientific and practical applications. Recently, periodic microstructures including photonic crystals have been shown to enable tuning of the spectral distribution of TR [1-5]. Furthermore, polarization properties of TR can be tuned by planar gratings [6,7], photonic crystals [8] and elongated nano-heaters [9]. These controls of spectral and polarization properties of TR are potentially very important especially for thermophotovoltaic devices. Tailoring the TR properties of the emitter to match the conversion characteristics of the photovoltaic cell [10] has the potential to greatly increase energy conversion efficiency. Moreover, the polarized TR source can also be extended to biological [11,12] and chemical applications as many chemical substances have linear-dichroic absorption [13]. Although highly polarized TR is simply possible by a flat metallic surface at grazing emergence [14] or even by using a polarizer with a conventional incandescent source, a major portion of supplied energy is inevitably wasted. In contrast, as the micro-structured polarized thermal-emitter (PTE) enables the polarized TR by selective radiation and not by filtering, the supplied energy can be used for desired TR with less loss.

Recently we found that TR from a layer-by-layer metallic photonic crystal with a homogeneous back-plane is not only spectrally enhanced but strongly polarized [16]. In this paper, we experimentally investigate variations of the layer-by-layer structure to be used as a PTE. The variations consist of two metallic grating layers having different periodicities; one of the gratings has sub-wavelength periodicity. In the experiment we observe that the PTE demonstrates a high extinction ratio close to 5 as well as a high emissivity in a mid-infrared range from 3 µm to 5 µm. As the range is tunable by adjusting structural parameters, the designed PTE will be very useful for improving the conversional efficiency of thermophotovoltaic devices.

2. Experiment

We fabricated three different layer-by-layer structures using the two-polymer microtransfer molding technique [5,17]. The scanning electron microscope (SEM) images of fabricated PTEs are shown in Fig. 1 with schematic illustrations of the structures. The PTEs are made of three components, two different gratings, "A" and "B", and a homogeneous back-plane, "C". The grating "A" consists of rods, 1.1 µm wide and 1.2 µm high, with 2.6 µm of rod-to-rod spacing and the grating "B" consists of rods, 0.6 µm wide and 0.4 µm high, with 1.0 µm of rod-to-rod spacing. One grating layer is perpendicular to the other and a monolithic and homogeneous nickel back-plane is usually added. We label the PTEs according to the order of the layers, as AAC (Fig. 1(a)), BAC (Fig. 1(b)), and ABC (Fig. 1(c)). In this study, we use the previously reported structure, AAC [16] as a reference. Each PTE is mounted on a heated copper block in a high vacuum chamber (~10^{-5} torr). Detailed information on the experimental setup is described in our previous report [5]. TR from PTE is collected at the surface normal angle with an acceptance angle of 5° and directed into a Fourier transform infrared spectrometer (Magna 760, Nicolet) then passed through a linear infrared polarizer (Spectra-Tech Inc.). A commercial blackbody source (M335, Mikron Infrared, Inc.) is used as a calibration source. The polarization angle of TR is set as zero when it is parallel to the orientation of a top grating layer as depicted in the schematic of Fig. 1.
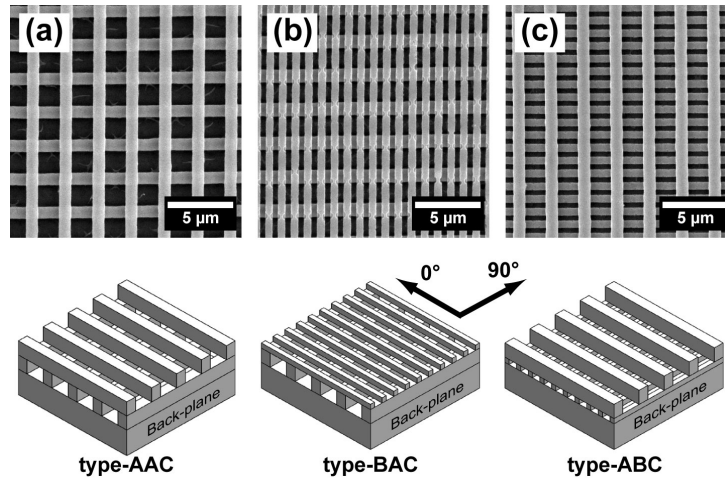
Fig. 1. SEM micrographs of the PTEs are shown with their diagrams of structures. The CPEs have three different configurations, (a) two identical gratings of "A"; (b) and (c) two different gratings of "A" and "B" with opposite orders of stacking. The polarization angle of TR is also graphically depicted.

The TR from the PTEs at a temperature of 800K is measured for two orthogonal polarization angles, parallel and perpendicular to the orientation of the top grating layer. The temperature of the PTE is determined to maximize the TR signals in the frequency range of interest. The measured TR power of each PTE is shown in Fig. 2 and all the three PTEs show very different TR characteristics. The BAC shows a single broad-peak only for a polarization angle of 90° while the AAC has sharp peaks for each polarization. In contrast the ABC has only minor peaks. The two adjacent peaks of the AAC in Fig. 2(a) are explained by degeneracy breaking in resonance modes of two identical gratings by interacting each other. Additionally the two-fold symmetry of each grating is still kept after stacking them, which is distinguishable from the 4-fold symmetry of a two-dimensional square lattice.
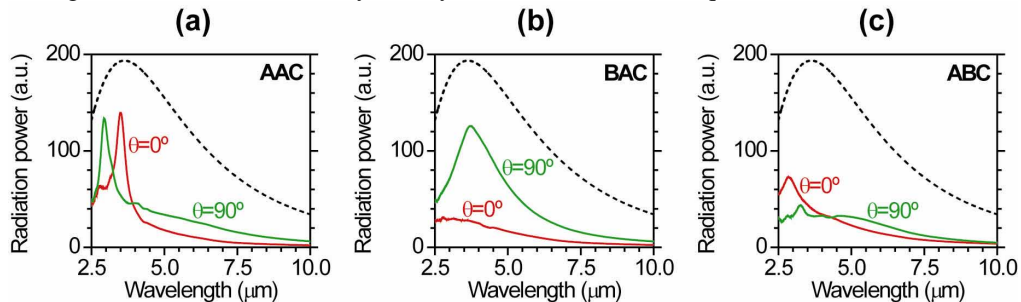

Fig. 2. Measured TR spectra of the PTEs at 800 K for the two polarization angles, parallel (red) and perpendicular (green) to the orientation of a top grating layer. (a) type-AAC; (b) type-BAC; (c) type-ABC. TR of a blackbody at the same conditions is plotted together (dashed).

The TR spectra yield corresponding emissivity spectra appear in Fig. 3(a). The measured wavelength range is divided into two regimes, resonance and non-resonance, as the measured TR characteristics are very different in the two regimes. In the non-resonance regime, the emissivities of 90°-polarization are observed to be higher than those of 0°-polarization for all PTEs. This is qualitatively explained by considering the top grating layer as a wire-grid polarizer. Since the transmission axis of the top grating layer is parallel to 90°-polarization angle, the TR from the second layer can contribute to the emissivity, in contrast to the TR of 0°-polarization. However, in the resonance regime when the wavelength of TR is comparable

to the feature size of the PTEs, the emissivity of 0°-polarization can be higher due to resonance effects.
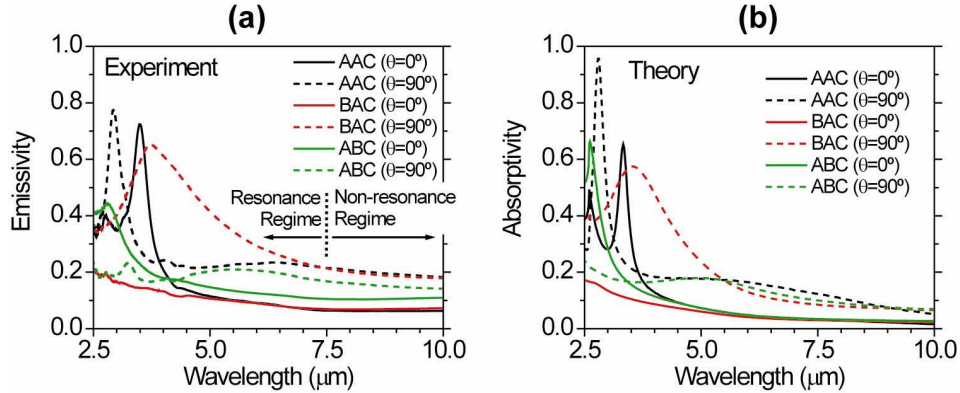

Fig. 3. (a) Measured emissivity spectra of the PTEs with (b) theoretically simulated absorptivity spectra.
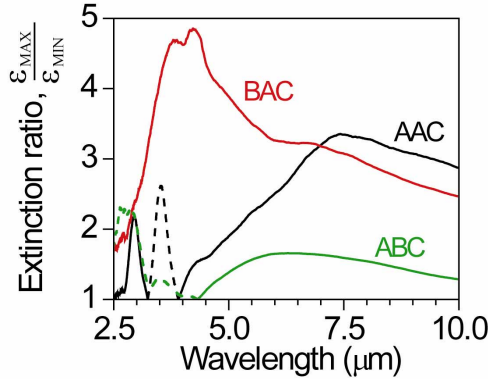

Fig. 4. The extinction ratio deduced from the measured spectral emissivities of the PTEs. Dashed lines represent that the dominant polarization is inverted, compared to that of the non-resonance regime.

It is interesting to compare the AAC and BAC as this can show how the emissivity can be tuned by changing the top layer from the grating "A" to the grating "B". We observed that the spectral emissivity of BAC is drastically changed from that of AAC in the resonance regime while they are almost identical in the non-resonance regime. The emission peak of AAC for 0°-polarization at 3.5µm has disappeared and the other peak of AAC for 90°-polarization at 3.0µm is shifted to 3.7µm for BAC. In addition to the shift, the width of the peak of AAC is broadened, approximately 5 times in full-width-at-half-maximum (FWHM), from FWHM of 0.42 µm to FWHM of 2.0 µm, where the FWHM is defined with a half emissivity, $\frac{1}{2}(\varepsilon_{peak} - \varepsilon_{10\mu m}) + \varepsilon_{10\mu m}$, where ε_{peak} and $\varepsilon_{10\mu m}$ are the values of emissivity at the peak and at a wavelength of 10µm, respectively. We note that an efficient polarized thermal emitter needs to have both a high emissivity and a high degree of polarization simultaneously. As the backplane boosts emissivity significantly at resonance wavelengths, the backplane makes the emitters more practical. Improved mechanical stability of the gratings at high temperature and convenience in attachment of the emitter to a heat source are other benefits of a backplane.

The absorptivity spectrum for each PTE is numerically calculated in Fig. 3(b) using a plane-wave-based transfer-matrix-method [18, 19]. In the calculation, reflectivity for normal incidence is calculated and subtracted from unity to yield absorptivity as the transmittance of the PTEs is zero due to the homogeneous back-plane "C". The calculated absorption spectra using the published optical parameters of nickel [20] show good agreement with the measured

emissivity spectra. The remaining minor deviations may be attributed to the difference in optical parameters of electroplated nickel used in the experiment from the published data and the temperature dependency of nickel [21]. As the simulated absorptivity represents the emissivity reasonably well, we will use the simulation for further analysis.

From the measured spectral emissivities, an extinction ratio, $\varepsilon_{max}/\varepsilon_{min}$, is plotted in Fig. 4, where ε_{max} and ε_{min} are the maximum and the minimum emissivities between the polarizations. The BAC shows an exceptionally high extinction ratio in the resonance regime, compared to the other two PTEs and the ratio approaches 5 at around 4 μm. Moreover, the dominant polarization is consistent in both resonance and non-resonance regimes while the dominant polarizations for the AAC and the ABC are reversed in the resonance regime. The electric-field (E-field) profiles of the BAC are numerically calculated for both polarizations to explain its high extinction ratio in Fig. 5.
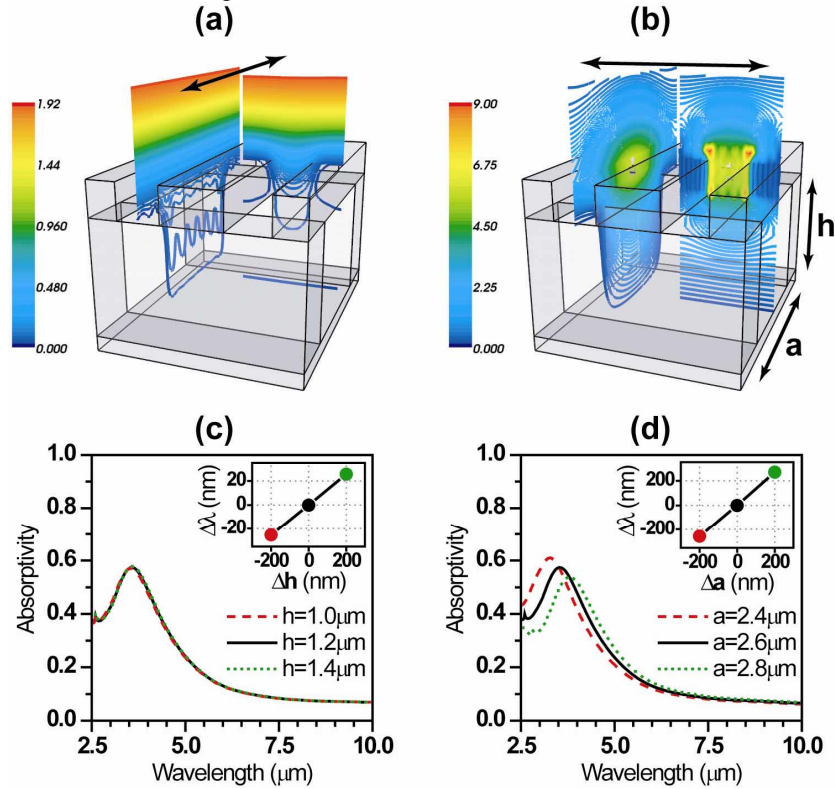

Fig. 5. E-field profiles of two unit-cells of the BAC structure are calculated at the wavelength of the peak for both polarizations (a) parallel and (b) perpendicular to the orientation of the top grating "B". The magnitudes of the electric field are normalized to that of the incident wave and depicted in different color scales to show the intensified electric field clearly. The arrows show the electric-field directions of incident waves in the calculations. The changes in absorptivity spectra as functions of (c) the height and (d) the periodicity of the grating "A" are also calculated. The insets are the shift of peaks versus variation in height or periodicity of the grating "A", respectively. The color of each marker is same as that of absorptivity spectrum.

As seen in Fig 5(a), the sub-wavelength grating "B" reflects the incident wave polarized parallel to its rods (θ=0°) and the magnitude of E-field outside is close to that of a non-structured nickel surface given by $1+\sqrt{R}$, where R is reflectivity of nickel (~0.91 at λ=3.5μm [20]). This means that grating "B" functions as a wire-grid polarizer. For the other polarization (θ=90°) in Fig. 5(b), a very high E-field exists within an air space surrounded by the two gratings, "A" and "B". The magnitude of the E-field in the middle of the air space is close to 6, in the other words, the enhancement in energy density is 9 times higher than the

possible enhancement by a flat metallic surface of the same material. We believe that the high E-field indicates a slowed group velocity for this range of wavelengths leading to enhancement of absorption. Figures 5(c) and 5(d) show the absorptivity spectra for the polarization (θ=90°) as functions of the height, h, and periodicity, a, of the grating "A". The absorptivity is not very sensitive to the layer height in the interested wavelength region. When the original height (1.2 µm) is changed ±200 nm, for example, spectral absorptivity is almost unchanged and the peak position shifts only ±25 nm, as shown in the inset of Fig. 5(c). In contrast, in Fig. 5(d), the absorptivity spectrum shifts as much as ±260 nm for the same amount of change, ±200 nm, in the periodicity of the grating "A". This shows that the air volume surrounded by the two gratings is more critical than the vertical air-gap between the top grating "B" and the back-plane "C". Figure 5(d) also show that the maximum value of the absorptivity increases as the periodicity is decreased. This trend is also the same for the periodicity of the top grating "B".

3. Conclusion

We fabricated metallic thermal emitters, consisting of two different nickel gratings on a homogeneous nickel layer, where one of the gratings has sub-wavelength periodicity. The metallic structure can enhance the emissivity of nickel in a certain range of wavelengths with a high degree of polarization. Our numerical simulations show that a high E-field is localized in the air space surrounded by the gratings for a specific polarization. We believe that the high E-field is induced by a polarization-sensitive group velocity and this is the major origin for the spectral enhancement of emissivity. Because the control of both spectral emissivity and polarization in thermal radiation is enabled, highly optimized thermal emitters for TPV and sensing applications are achievable.